Available online at www.sciencedirect.com
ScienceDirect
International Journal of Heat and Mass Transfer 50 (2007) 5241–5248
International Journal of HEAT and MASS TRANSFER
www.elsevier.com/locate/ijhmt

Thermo-optical modeling of polymer fiber Bragg grating illuminated by light emitting diode

Kyoung Joon Kim, Avram Bar-Cohen *, Bongtae Han

Department of Mechanical Engineering, University of Maryland, College Park, MD 20742, USA

Received 28 September 2005; received in revised form 1 June 2006
Available online 5 September 2007

Abstract

The development of a thermo-optical model of an illuminated polymer fiber Bragg grating (PFBG), combining use of the modified coupled-mode theory with thermal conduction theory and the modified transfer matrix method (TMM), is presented. This model is applied to the prediction of the thermo-optical behavior of an intrinsically heated and passively cooled PMMA fiber Bragg grating illuminated with a LED light source and operating over a range of ambient temperatures. Parametric influences on the thermo-optic characteristics and the predictive accuracy of several simplifications in the Bragg grating relations are also explored.

Keywords: Thermo-optical modeling; Polymer fiber Bragg grating; Light emitting diode; Bragg wavelength

1. Introduction

Polymer components are of growing interest in the optical engineering community and while polymer waveguides are currently receiving much of the attention [1], polymer Bragg gratings (BGs) have been proposed as passive filters [2], tuning filters [3], WDM systems [4], and couplers [5]. Bragg gratings (BGs) are passive optical components used in light transmitting waveguides to produce a very narrow band of reflected optical energy, with a maximum reflectivity at the characteristic wavelength of the grating, called the *Bragg wavelength*. Such a grating can be formed by refractive index modulations in an optical fiber to form a so-called Fiber Bragg grating (FBG), as illustrated in Fig. 1. When used in conjunction with a broad-band light emitting diode (LED), typically emitting light over a spectral range of 100 nm, a BG filter can produce a narrow-band reflection just 0.1 nm wide, centered on a specific wavelength. However, the temperature sensitivity of the properties of candidate polymer photonic materials, coupled with the self-heating generated by the intrinsic light absorption of these materials, can alter the spectral characteristics of the reflected and transmitted light waves in such a BG. A detailed understanding of the thermo-optic behavior of polymer Bragg Gratings is required to rationalize the grating design and to facilitate the selection (or creation) of the most suitable polymeric materials for a specified functional capability.

2. Light absorption in polymer Bragg gratings

2.1. Optics of Bragg gratings

The light power incident on a fiber Bragg Grating can typically be assumed to follow a radial Gaussian profile and to be given by [6]

$$I(r) = \frac{2P_{\text{inc}}}{\pi w^2} e^{-2r^2/w^2} \tag{1}$$

where P_{inc} is the incident total optical power and w is the beam radius [6].

* Corresponding author. Tel.: +1 301 405 3173; fax: +1 301 314 9477.
E-mail address: abc@umd.edu (A. Bar-Cohen).

0017-9310/$ - see front matter © 2007 Elsevier Ltd. All rights reserved.
doi:10.1016/j.ijheatmasstransfer.2007.06.038

Nomenclature

a	dB-based intrinsic absorption coefficient (dB/cm)
$\hat{a}$	intrinsic absorption coefficient (m^{-1})
h	effective heat transfer coefficient (W/m^2 K)
h_{cl}	total combined (convection and radiation) heat transfer coefficient at optical fiber surface (W/m^2 K)
$I(r)$	radial variation of power irradiance ($mW/\mu m^2$)
k	thermal conductivity (W/m K)
L	total grating length (cm)
m	eigen value of coupled-mode equations
n	refractive index
n_{eff}	effective refractive index
dn/dT	thermo-optical coefficient (K^{-1})
P_{inc}	incident total optical power (mW)
$P(\lambda, r, z)$	distribution of optical power ($mW/nm\ \mu m^2$)
$\overline{P(\lambda)}$	normalized spectral power density
$P_i(\lambda)$	incident power spectrum (mW/nm)
$P_{ref}(\lambda)$	reflected power spectrum (mW/nm)
$q_G(r,z)$	heat generation (W/cm^3)
$R(z)$	amplitude of forward traveling wave
$\lvert R\rvert^2$	power of forward traveling wave
$\lvert R\rvert^2_M$	power of forward traveling wave, calculated by transfer matrix method, at inlet of PFBG
r_{co}	radius of fiber core (μm)
r_{cl}	radius of entire fiber (μm)
r_o	the radius of a volume which contains total incident optical power (μm)
$S(z)$	amplitude of backward traveling wave
$\lvert S\rvert^2$	power of backward traveling wave
$\lvert S\rvert^2_M$	power of backward traveling wave, calculated by transfer matrix method, at inlet of PFBG
T	temperature (K)
w	beam radius (μm)
r, z	geometrical coordinates

Greek symbols

α	coefficient of thermal expansion (K^{-1})
Δ	amount of change relative to reference
δ	detuning value (nm^{-1})
Δn_{eff}	index modulation for grating
θ	excess temperature above ambient (K)
θ_o	excess temperature at inlet of PFBG (K)
κ	coupling coefficient (m^{-1})
Λ	grating period (nm)
λ	wavelength of incident light (nm)
λ_B	Bragg wavelength (nm)
$\Delta\lambda_B$	Bragg wavelength shift (nm)
λ_c	central wavelength of light source (nm)
$\Delta\lambda_c$	half of total spectral bandwidth (nm)
$\rho(\lambda)$	reflectivity spectrum
ρ_{max}	maximum reflectivity
$\hat{\sigma}_j$	'dc' coupling coefficient for a specified element in transfer matrix method (m^{-1})

Subscripts

B	Bragg condition
c	center of wavelength window
cl	cladding of optical fiber
co	fiber core
eff	effective
inc	incident
o	the outer surface of the volume which contains a total incident optical power

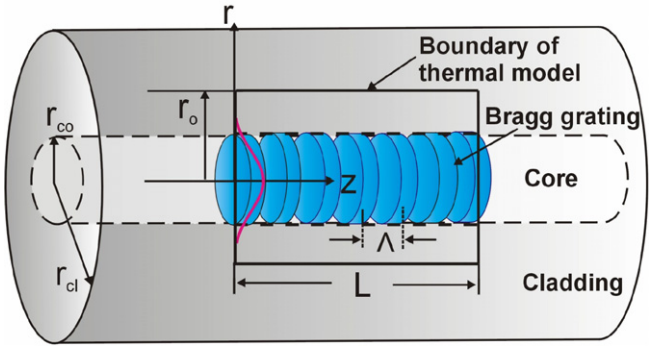

Fig. 1. Geometry of polymer fiber Bragg grating thermal model.

Similarly, engineering data [7,8] for typical light sources of interest, suggests that the power spectrum often follows a Gaussian wavelength distribution. The spectral power density normalized by the power at the peak wavelength, $\overline{P(\lambda)}$, for such light sources can, thus, be expressed as

$$\overline{P(\lambda)} = B e^{4\ln 0.5((\lambda-\lambda_c)/\mathrm{FWHM})^2} \tag{2}$$

$$\text{where } B = \frac{1}{2\int_0^{\Delta\lambda_c} e^{4\ln 0.5((\lambda-\lambda_c)/\mathrm{FWHM})^2}\, d(\lambda)} \tag{3}$$

where λ_c is the central wavelength of the light source, $\Delta\lambda_c$ (equal to $\lambda - \lambda_c$) is half of the total spectral bandwidth and FWHM is the "full width half maximum", which defines the spectral bandwidth at half the maximum power.

When light is incident on the fiber grating, the refractive index modulation results in the reflection of a narrow bandwidth of light, centered around the Bragg wavelength, λ_B, defined by the effective refractive index and period of the grating as [9]

$$\lambda_B = 2 n_{eff} \Lambda \tag{4}$$

where n_{eff} is the effective refractive index, which is the index of the guided mode through the fiber and depends on the indices of core and cladding, and Λ is the grating period. It is the temperature sensitivity of the effective refractive index, n_{eff}, and the thermal-expansion driven change in the

grating pitch, Λ, that together are responsible for the thermo-optic sensitivity of a polymer Bragg grating.

For light wavelengths sufficiently removed from the Bragg wavelength, i.e. large values of $|\lambda - \lambda_B|$, the BG reverts to a simple waveguide, producing no reflection. For wavelengths in close proximity to λ_B the optical characteristics of the BG, including the reflection spectrum and the reflectivity, can be predicted well by the coupled-mode theory [9–12]. Following Kogelnik [10,11], with some adjustment for the present nomenclature and coordinate system, the z-direction derivatives of the amplitudes of the incident (forward moving) and reflected (backward moving) waves can be expressed in the form of the "coupled-mode" equations [9,10], i.e.

$$\frac{dR}{dz} = -i\hat{\sigma}R(z) - i\kappa S(z) \tag{5}$$

$$\frac{dS}{dz} = i\hat{\sigma}S(z) + i\kappa R(z) \tag{6}$$

where $R(z)$ and $S(z)$ are the amplitudes of the forward traveling and backward traveling waves, respectively, the 'dc' self-coupling coefficient, $\hat{\sigma}$, is related to the detuning parameter, δ, and the intrinsic absorption coefficient, $\hat{a}$, according to

$$\hat{\sigma} = \delta - \frac{\hat{a}}{2}i \tag{7}$$

and κ is the coupling coefficient [9]. It is to be noted that $\hat{a}$ (m^{-1}), as used in the present analysis, is related to the more common dB-based absorption coefficient, a (dB/cm) by the following relation:

$$\hat{a} = 10 \cdot a \ln(10) \tag{8}$$

The detuning value is a measure of the spectral proximity of the incident light to the Bragg wavelength, and is defined as [9]

$$\delta = \frac{2\pi n_{eff}}{\lambda} - \frac{\pi}{\Lambda} \tag{9}$$

Following the procedure in [10], the closed form solutions of the coupled-mode equations can be written as

$$R = r_1 e^{mz} + r_2 e^{-mz} \tag{10}$$

$$S = s_1 e^{mz} + s_2 e^{-mz} \tag{11}$$

where the Eigen value of the coupled-mode equations is

$$m = \sqrt{\kappa^2 - \hat{\sigma}^2} \tag{12}$$

and is, thus, dependent on the absorption coefficient, the detuning value, and the coupling coefficient. Using these relations, with boundary conditions which set the amplitude of the forward wave at the inlet to unity and the amplitude of the backward moving wave at the outlet to zero ($R(0) = 1$ and $S(L) = 0$), and multiplying the conjugates of the complex amplitudes of two waves, the axial power of the forward and the backward moving waves respectively, can be found [13].

Graphs of the axial power variation for the forward and backward moving waves in a typical optical polymer (PMMA) FBG (properties shown in Table 1) for several distinct values of $|\lambda - \lambda_B|$ with 0.001 nm steps, are displayed in Fig. 2. The graphs reveal the expected behavior at the Bragg wavelength and show the effects of diminished coupling – on the slope and magnitude of the power graphs – for increasing values of $|\lambda - \lambda_B|$. For large values of $|\lambda - \lambda_B|$ the BG reverts to a simple waveguide, producing no reflection, and yielding an exponentially decaying, axial power distribution as represented by Beer's law [6].

To determine the power propagating in a BG illuminated by a specified light source, it is necessary to integrate the optical power, $P(\lambda, r, z)$, across the bandwidth of the light source, including both the Bragg zone, where intense interaction and strong reflection will occur, and the wave-

Table 1
Properties and geometry of PMMA fiber Bragg grating

Parameter	Symbol	Value
Basic parameters [14–16]		
Radius of core	r_{co}	3.5 μm
Length	L	1 cm
Grating period	Λ	530.7 nm
Refractive index of core	n_{co}	1.49
Refractive index of cladding	n_{cl}	1.48
Bragg wavelength	λ_B	1576.5 nm
Maximum reflectivity without absorption	ρ'_{max}	0.8
Derived parameters		
Effective refractive index	n_{eff}	1.4853
Coupling coefficient at Bragg wavelength	κ_B	144.36 m^{-1}
Index modulation	δn_{eff}	7.244×10^{-5}
Maximum reflectivity with absorption	ρ_{max}	0.745
Beam radius	w	3.7402 μm
Material properties of PMMA [17]		
Thermal conductivity	k	0.2 W m^{-1} K
Coefficient of thermal expansion	α	73×10^{-6} K^{-1}
Absorption coefficient	$\hat{a}$	11.513 m^{-1}
Thermo-optical coefficient	dn/dT	-1.1×10^{-4} K^{-1}

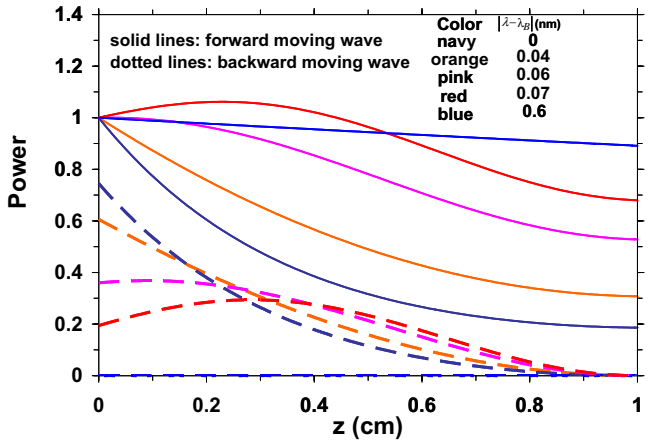

Fig. 2. Coupled-mode solution for incident and reflected power along PMMA fiber Bragg grating.

guide zone, where the presence of the grating has no effect on the traversing light. While a typical narrow-band single mode laser diode (SMLD), with a FWHM of 20 pm, may operate entirely in the Bragg zone, the vast majority of the light from a broad-band LED light source (with a FWHM of 50 nm) would be far removed form the Bragg wavelength and subject only to Beer's Law of propagation.

2.2. Non-uniform grating pitch

The generally exponential axial variation of the propagating power and, hence, internal heat generation can be expected to yield a similar exponential axial variation in temperature in the PFBG and to thus lead to a non-uniform grating pitch and effective index and, hence, non-uniform detuning. The transfer matrix method (TMM) can be used for determining the optical field in a Bragg grating with a non-uniform detuning [9,18,19]. Following the TMM, the optical characteristics of each small segment, F_j, of a BG can be linearly coupled to the next segment and can be represented in a matrix form as [9,18,19]

$$\begin{bmatrix} R_M(\lambda) \\ S_M(\lambda) \end{bmatrix} = F(\lambda) \begin{bmatrix} R(L) \\ S(L) \end{bmatrix};$$
$$F(\lambda) = F_M(\lambda) \cdot F_{M-1}(\lambda) \cdot \cdot F_j(\lambda) \cdot \cdot F_1(\lambda) \tag{13}$$

In the TMM, at the end of the grating, unity and zero are assumed for the forward and the backward moving waves' amplitude, i.e. $R(L) = 1$ and $S(L) = 0$, to obtain the amplitudes of both waves at the inlet of the grating. Each of the divided segments, $F_j(\lambda)$, with a grating length of Δz, must satisfy the coupled-mode theory, which results in the following mathematical description [9,18,19]

$$F_j(\lambda) = \begin{bmatrix} -\cosh(m_j(\lambda)\Delta z) - \mathrm{i}\frac{\hat{\sigma}_j(\lambda)}{m_j(\lambda)}\sinh(m_j(\lambda)\Delta z) & -\mathrm{i}\frac{\kappa(\lambda)}{m_j(\lambda)}\sinh(m_j(\lambda)\Delta z) \\ \mathrm{i}\frac{\kappa(\lambda)}{m_j(\lambda)}\sinh(m_j(\lambda)\Delta z) & -\cosh(m_j(\lambda)\Delta z) + \mathrm{i}\frac{\hat{\sigma}_j(\lambda)}{m_j(\lambda)}\sinh(m_j(\lambda)\Delta z) \end{bmatrix} \tag{14}$$

where the coupling coefficient, $\kappa(\lambda)$, is again equal to $\pi \cdot \Delta n_{\mathrm{eff}}/\lambda$, and Δn_{eff} to the index modulation of the grating. While $F_j(\lambda)$ is fundamentally identical to the transfer matrix presented in [9], it should be noted that components of $F_j(\lambda)$ were formulated to satisfy the present nomenclature and coordinate system.

3. Self-heating in polymer Bragg gratings

3.1. Intrinsic absorption

Having established the power variation in the Bragg grating, it is now possible to determine the heating rate induced by the intrinsic absorption in the fiber, by an appropriate convolution of the power functions and absorption coefficients. Since for a LED source, nearly all of the illumination is external to the Bragg zone, heat generation can be determined by application of Beer's Law and the solution of the thermal field can, then, precede and be separate from, the solution of the coupled-mode equations.

Assuming the absorption coefficient to be constant along the length and radius of the grating, as well as to be invariant with wavelength, the internal heat generation rate in the PFBG can be found by a very good approximation, by assuming simple absorption across the full bandwidth of the source, i.e.

$$q_G(r,z)|_{\mathrm{LED}} = I(r)\mathrm{e}^{-\hat{a}z} \cdot \hat{a} \tag{15}$$

3.2. Bragg wavelength shift

3.2.1. Uniform grating temperature

Returning to Eq. (4), the Bragg wavelength of an intrinsically heated polymer fiber grating, λ_{B2}, can be written as

$$\lambda_{\mathrm{B2}} = \lambda_{\mathrm{B1}} + \Delta\lambda_{\mathrm{B}} = 2(n_{\mathrm{eff}_1} + \Delta n_{\mathrm{eff}})(\Lambda_1 + \Delta\Lambda) \tag{16}$$

where subscript '1' denotes the initial state and '2' the changed state.

Assuming that the dependence of the effective index of refraction on temperature is constant, i.e. $\mathrm{d}n/\mathrm{d}T = \text{constant}$, and that the core and cladding display similar rates of change, the index change caused by self-heating, Δn_{eff}, can be expressed as

$$\Delta n_{\mathrm{eff}} = \frac{\mathrm{d}n}{\mathrm{d}T}\Delta T \tag{17}$$

The change of the grating period due to thermal expansion is given as

$$\Delta\Lambda = \Lambda\alpha\Delta T \tag{18}$$

Substituting Eqs. (17) and (18) into Eq. (16), one can get

$$\lambda_{\mathrm{B2}} = 2\left(n_{\mathrm{eff}_1} + \frac{\mathrm{d}n}{\mathrm{d}T}\Delta T\right)(\Lambda_1 + \Lambda_1\alpha\Delta T) \tag{19}$$

Subtracting the expression for λ_{B1} and dividing both sides of Eq. (19) by λ_{B1}, the analytical relation for the normalized Bragg wavelength shift, $\Delta\lambda_{\mathrm{B}}/\lambda_{\mathrm{B1}}$, can be expressed as

$$\frac{\Delta\lambda_{\mathrm{B}}}{\lambda_{\mathrm{B1}}} = \left(\frac{1}{n_{\mathrm{eff}_1}}\frac{\mathrm{d}n}{\mathrm{d}T} + \alpha\right)\Delta T + \left(\frac{1}{n_{\mathrm{eff}_1}}\frac{\mathrm{d}n}{\mathrm{d}T} \cdot \alpha\right)\Delta T^2 \tag{20}$$

where $\Delta\lambda_{\mathrm{B}} = \lambda_{\mathrm{B2}} - \lambda_{\mathrm{B1}}$.

Eq. (20) provides a two-term relation for the normalized Bragg wavelength shift; the first involving a linear dependence and the second a quadratic dependence on the temperature rise.

For typical glassy polymers used for optical fibers operating at 1550 nm with an index of refraction of 1.5, the $\mathrm{d}n/\mathrm{d}T$ is negative and falls in the range of 100–200 $\times 10^{-6}$/K,

while the thermal-expansion coefficient, α, is positive and can be expected to range from 60 to 80×10^{-6}/K [17]. Due to the relatively large thermal-expansion coefficient of the PFBG and the relatively small difference between the negative thermo-optic effect and positive grating period effect in the linear ΔT term, this quadratic term cannot generally be neglected in the analysis of polymer PFBG, though it is negligible for glass FBG, for which the product of α and dn/dT is far smaller than the sum [20].

3.2.2. Non-uniform grating temperature

The absorption-induced self-heating of the PFBG generates an axially exponential temperature profile, and results in non-uniform index and grating period along the PFBG. Consequently, the F-matrix, F_j, in the transfer matrix must be modified to include the effect of these thermally induced non-uniformities on the optical behavior of the PFBG. Considering the thermally driven index shift, the "new" index of refraction for each segment of the grating, $n_{\mathrm{eff}_{2,j}}$ can be expressed as

$$n_{\mathrm{eff}_{2,j}} = n_{\mathrm{eff}_1} + \frac{dn}{dT}\Delta T_j \tag{21}$$

Similarly, the "new" period of the grating element caused by thermal expansion is

$$\Lambda_{2,j} = \Lambda_1(1 + \alpha \Delta T_j) \tag{22}$$

Using Eqs. (21) and (22), the 'dc' coupling coefficient for a specified element, $\hat{\sigma}_j$, can be written as

$$\begin{aligned}\hat{\sigma}_j(\lambda) &= \frac{2\pi n_{\mathrm{eff}_j}}{\lambda} - \frac{\pi}{\Lambda_j} - \mathrm{i}\frac{\hat{a}}{2} \\ &= \frac{2\pi}{\lambda}\left(n_{\mathrm{eff}_1} + \frac{dn}{dT}\Delta T_j\right) - \frac{\pi}{\Lambda_1(1+\alpha\Delta T_j)} - \mathrm{i}\frac{\hat{a}}{2}\end{aligned} \tag{23}$$

and the Eigen value of coupled-mode equations, m_j, can be expressed as

$$\begin{aligned}m_j(\lambda) &= \sqrt{\kappa^2(\lambda) - \hat{\sigma}_j^2(\lambda)} \\ &= \sqrt{\left(\frac{\pi}{\lambda}\Delta n_{\mathrm{eff}}\right)^2 - \left(\frac{2\pi}{\lambda}\left(n_{\mathrm{eff}_1} + \frac{dn}{dT}\Delta T_j\right) - \frac{\pi}{\Lambda_1(1+\alpha\Delta T_j)} - \mathrm{i}\frac{\hat{a}}{2}\right)^2}\end{aligned} \tag{24}$$

Substituting $\hat{\sigma}_j$ and m_j into Eq. (14), defines all the terms of the matrix, F_j.

Using the boundary condition ($R(L) = 1$ and $S(L) = 0$) [9,18,19], the reflectivity spectrum can then be found as

$$\rho(\lambda) = \frac{|S_M(\lambda)|^2}{|R_M(\lambda)|^2} \tag{25}$$

With the reflectivity determined, it is possible to obtain the reflected power spectrum, $P_{\mathrm{ref}}(\lambda)$, as the product of the incident optical power and the reflectivity. Mathematically, it can be expressed in a simple form as

$$P_{\mathrm{ref}}(\lambda) = P_i(\lambda)\overline{P(\lambda)}\rho(\lambda) \tag{26}$$

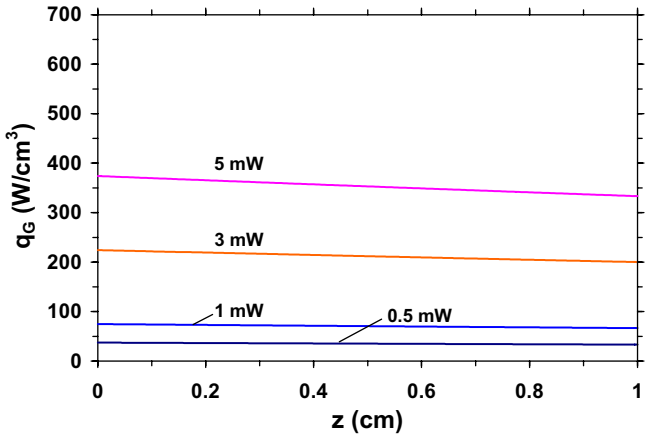

Fig. 3. Heat generation densities along a PMMA fiber Bragg grating illuminated by light emitting diode (LED).

4. Thermo-optical behavior of LED illuminated PMMA FBG

4.1. Introduction

As a first illustration of the thermo-optical behavior of an intrinsically heated polymer Bragg grating, attention will now be focused on a polymethylmetacrylate (PMMA) FBG, described in the literature [14–16], illuminated with a broad-band LED light source, with a central wavelength of 1550 nm and 50 nm of FWHM [8], some 50–100 times larger than a typical grating bandwidth. Table 1 shows all the inherent and derived parameters of the chosen PFBG, including the material properties and the structural, as well as optical parameters. The Bragg wavelength (λ_B), the grating period (Λ), the effective index (n_{eff}), the maximum reflectivity ($\rho_{\max}$), and the absorption coefficient ($\hat{a}$) are 1576.5 nm, 530.7 nm, 1.4853, 0.745, and 11.513 m^{-1}, respectively.

4.2. Power/heat generation variation along PMMA FBG

For the broad-band illumination provided by the LED, extending substantially beyond the 0.6 nm bandwidth of the PFBG, to 1576 nm ± 100 nm (for 48 dB down from the peak power), heat generation in the fiber can be determined from the inherent absorption of the propagating beam, using Eq. (15). The resulting exponentially decaying axial profile of heat generation along the PFBG is shown in Fig. 3 for four different incident optical powers of 0.5, 1, 3, and 5 mW, reflecting the impact of the 11% light absorption in the 1 cm long fiber. It should be noted that the heat generation rates along the PFBG are significant, ranging from 30 W/cm^3 to 370 W/cm^3 for 0.5 to 5 mW of incident total optical power.

4.3. Thermal analysis

Determination of the steady-state temperature field in the intrinsically heated PFBG requires solution of the heat

conduction equation with non-uniform heat generation. Since the fiber Bragg grating length is much larger than the core diameter, with a typical aspect ratio greater than 100 [19], it is possible to neglect radial variations in heat generation and temperature and to reduce the governing equation to a one-dimensional heat conduction equation. Inserting the relation for the internal heat generation (Eq. (15)) for the broad-band LED light source, the one-dimensional heat conduction equation [21] takes the form of

$$\frac{\mathrm{d}^2\theta}{\mathrm{d}z^2} - p^2\theta = \frac{-P_{\mathrm{inc}}}{k\pi r_{\mathrm{o}}^2}\cdot \mathrm{e}^{-\hat{a}z}\cdot \hat{a} \tag{27}$$

where $p = \sqrt{2h/(kr_{\mathrm{o}})}$, θ is the excess temperature above ambient, and k is the thermal conductivity.

A schematic of the domain and symbols used for the analytical thermal model are shown in Fig. 1, where r_{co} is the radius of the fiber core, r_{cl} is the radius of the entire fiber including its cladding, r_{o} is the radius of a volume which contains the total incident optical power, Λ is the grating period, and L is the total length of the grating. In the above equation, h is the effective heat transfer coefficient on the outer surface of the modeled volume, reflecting the conductive resistance to heat flow through the cladding and the convective and radiative resistance between the exposed surface and the ambient, which can be expressed as [22]

$$h = \frac{1}{\frac{r_{\mathrm{o}}}{k}\ln\frac{r_{\mathrm{cl}}}{r_{\mathrm{o}}} + \frac{r_{\mathrm{o}}}{h_{\mathrm{cl}}r_{\mathrm{cl}}}} \cong \frac{r_{\mathrm{cl}}}{r_{\mathrm{o}}}h_{\mathrm{cl}} \tag{28}$$

where h_{cl} is the total combined (convection and radiation) heat transfer coefficient at the optical fiber surface. For the dimensions and conductivity of typical polymer optical fibers, the conductive term $(r_{\mathrm{o}}/k\cdot\ln(r_{\mathrm{cl}}/r_{\mathrm{o}}))$ can be neglected relative to the convective/radiative term $(r_{\mathrm{o}}/(h_{\mathrm{cl}}r_{\mathrm{cl}}))$ in the denominator of Eq. (28), yielding the approximation shown. For purposes of this analysis, the outer surface of the fiber was assumed to be passively cooled by natural convection and radiation, with an approximate heat transfer coefficient of $10\ \mathrm{W/m^2\,K}$. Consequently, it can be shown that when r_{o}, r_{cl}, and k are 7 μm, 50 μm, and 0.2 W/m K, respectively, $r_{\mathrm{o}}/(h_{\mathrm{cl}}r_{\mathrm{cl}})$ is equal to 1.4×10^{-2}.

The general solution of Eq. (27) can be written as

$$\theta = d_1\mathrm{e}^{pz} + d_2\mathrm{e}^{-pz} + \theta_s \tag{29}$$

The particular solution can be expected to take the form of

$$\theta_s = D\mathrm{e}^{-\hat{a}z} \tag{30}$$

Assuming that both ends of the PFBG are adiabatic, i.e. $\mathrm{d}\theta/\mathrm{d}z = 0$ at $z = 0$ and $z = L$ and that all heat loss occurs from the surface of the fiber the axial temperature variation in the PFBG is found as

$$\theta = \frac{P_{\mathrm{inc}}\hat{a}^2}{\pi r_{\mathrm{o}}^2 k\cdot(p^2-\hat{a}^2)}\left\{\frac{\mathrm{e}^{-\hat{a}L}\cosh(pz) - \cosh[p(z-L)]}{p\sinh(pL)} + \frac{\mathrm{e}^{-\hat{a}z}}{\hat{a}}\right\} \tag{31}$$

where for polymer optical fibers, p is typically two orders of magnitude greater than $\hat{a}$ due to the micron-size diameter of the fiber core. Hence, the equation can be further simplified by neglecting, $\hat{a}^2$, in the denominator as

$$\theta = \frac{P_{\mathrm{inc}}\hat{a}^2}{\pi r_{\mathrm{o}}^2 k p^2}\left\{\frac{\mathrm{e}^{-\hat{a}L}\cosh(pz) - \cosh[p(z-L)]}{p\sinh(pL)} + \frac{\mathrm{e}^{-\hat{a}z}}{\hat{a}}\right\} \tag{32}$$

Examining Eq. (32), it may be seen that the temperature can be expected to decay exponentially in the axial direction, increase with incident power and the absorption coefficient, and decrease with thermal conductivity.

4.4. Temperature profiles

Fig. 4 shows the PFBG axial profiles of the excess temperature (determined relative to a 25 °C ambient) for the four incident optical powers. The fiber excess temperatures vary from 18 K at the inlet of the fiber illuminated with the highest incident power of 5 mW to just 2 K for 0.5 mW of illumination. The analytical results display the anticipated, though weak exponential decay in temperature and appear to match FEA modeling results for this PFBG [13] typically to within 0.7%.

The finite-element model was further utilized to compute the radial temperature variations in the PFBG. The results are shown in Fig. 5, where the axial variation of the temperature difference $(T_{\mathrm{c}} - T_{\mathrm{co}})$ between the center of the PFBG core (T_{c}) and the core surface (T_{co}) is plotted. The peak radial temperature differences are seen to range from 0.06 K at 5 mW to 0.01 K at 0.5 mW of incident LED power and to thus justify the radially uniform temperature assumption used in the analytical temperature relations. Fig. 5 also reveals a slight decrease in the radial temperature difference as the PFBG is traversed from the inlet to the outlet end.

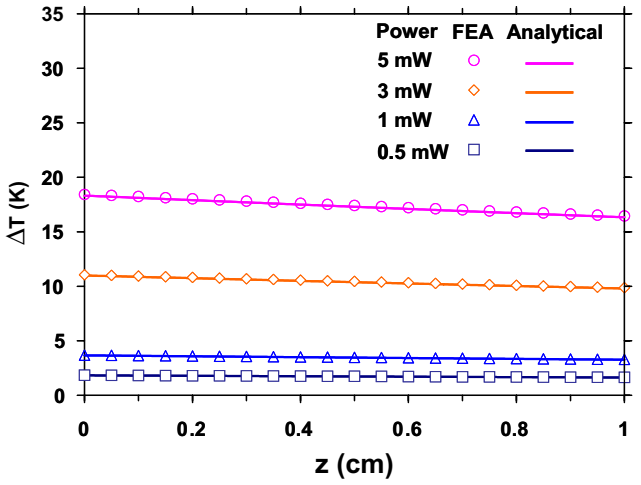

Fig. 4. Analytical and numerical excess temperatures along PMMA fiber Bragg grating illuminated by light emitting diode.

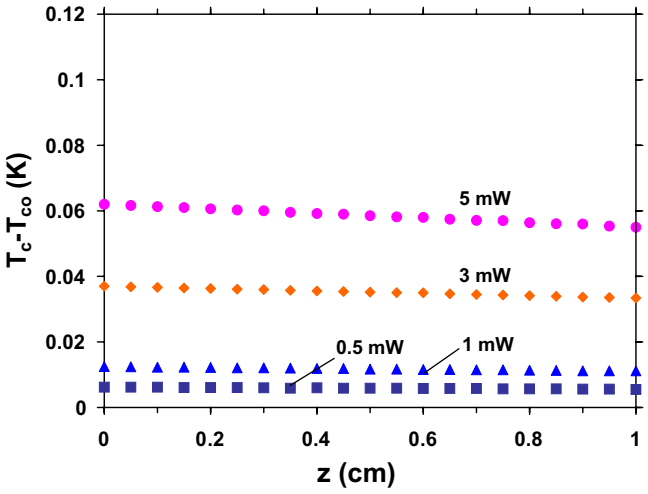

Fig. 5. Radial temperature differences along PMMA fiber Bragg grating illuminated by light emitting diode.

4.5. Spectral distribution

In order to obtain the reflectivity spectrum of the specified PFBG associated with the LED, the temperature distribution obtained from Eq. (32) was integrated with the modified TMM relations (Eqs. (13) and (14)). In the TMM implementation, a total of 200 segments, each 50 μm wide, was used, along with wavelength bands of 0.5 pm. Fig. 6 displays the thermally induced shift in the spectral reflectivity of the specified PFBG illuminated with 5–0.5 mW of LED powers and operating in an ambient temperature of 25 °C. The individual effects of the index change with temperature (dn/dT), and the grating period change with temperature ($d\Lambda/dT$), were determined.

The results clearly indicate that the thermally driven index change produces a negative shift in the reflectivity spectrum, relative to the incident 1576.5 nm-centered LED light. At 5 mW of the LED illumination, the dominant "Bragg" wavelength moves lower by −2.03 nm as shown in Fig. 6a. The change of the grating period due to thermal-expansion results in a positive shift in the reflectivity spectrum, driving the dominant wavelength to higher values by 2.0 nm. The combined reflectivity spectrum for the 5 mW illuminated fiber shows a very small total shift in Bragg wavelength (−0.03 nm), with modest spectral dispersion. Fig. 6b–d shows the individual and the combined reflectivity spectrums for 3–0.5 mW of the LED illuminations, revealing similarly small total shifts in Bragg wave-

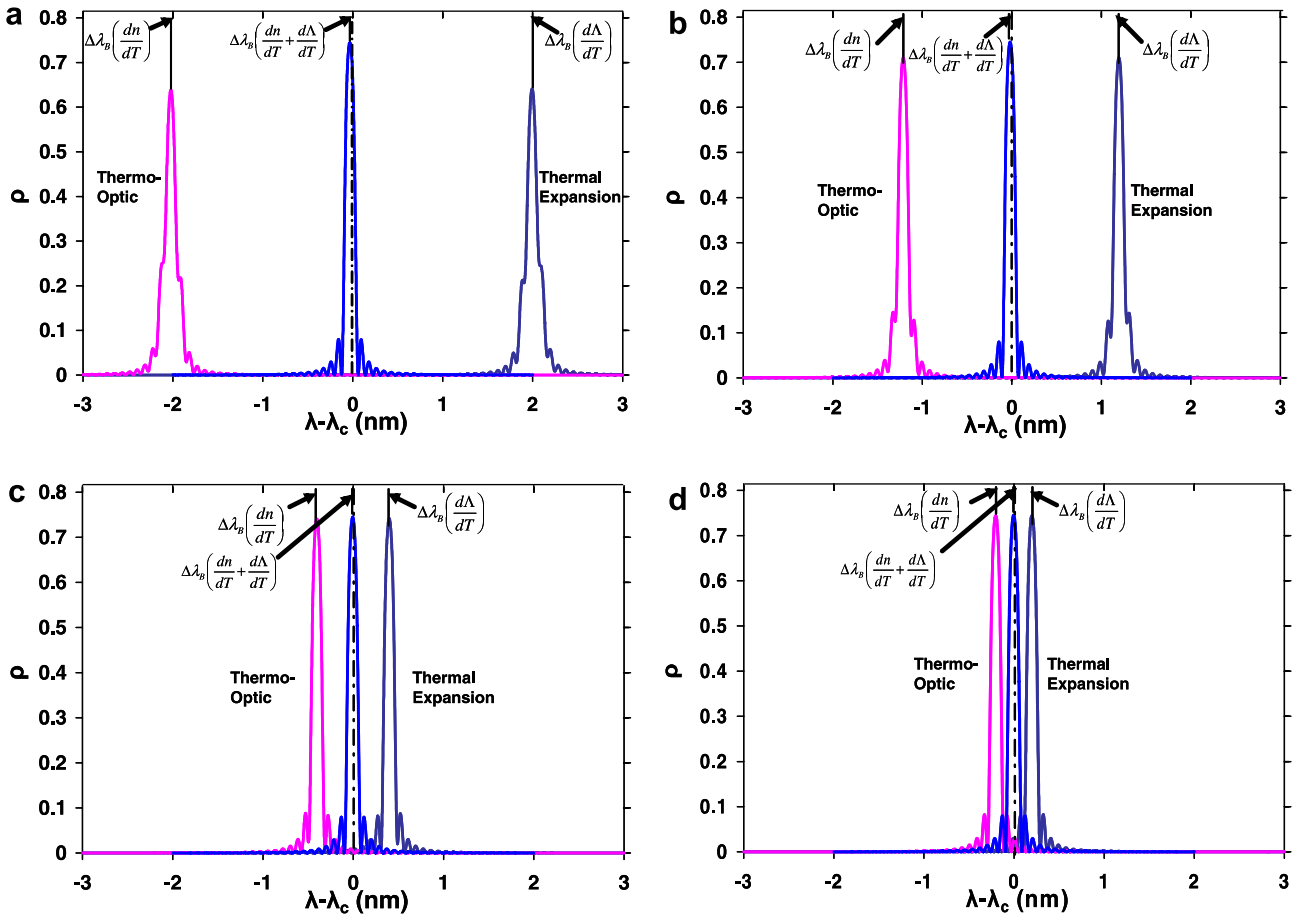

Fig. 6. Thermally induced Bragg wavelength shifts in PMMA fiber Bragg grating illuminated with a light emitting diode – thermo-optic (dn/dT), thermal expansion ($d\Lambda/dT$), and combined effects ($dn/dT + d\Lambda/dT$) are shown for (a) 5 mW, (b) 3 mW, (c) 1 mW, and (d) 0.5 mW of incident optical power.

length of −0.02 nm, −0.006 nm, and −0.003 nm for 3 mW, 1 mW, and 0.5 mW of the total optical power, respectively. The jagged character of the reflectivity spectrum is associated with the spectral dispersion induced by the axially non-uniform PFBG temperature and will be explored in depth in a subsequent publication.

The Bragg wavelength shift in an illuminated PFBG is driven by the temperature change in the PFBG induced by both absorption and ambient temperature changes. The Bragg wavelength shifts were evaluated using both the modified-TMM and the analytic relation (Eq. (20)), with an axially averaged PFBG temperature, and detailed results can be found in [13].

The significant effect of ambient temperature on the shift in Bragg wavelength was found to be evident; a 15 K ambient temperature rise yielded a $\Delta\lambda_B$ almost equivalent to that of the incident power increased from 0.5 mW to 5 mW [13].

5. Summary

The modified coupled-mode theory has been combined with thermal conduction theory and the modified transfer matrix method (TMM) to study the thermo-optical behavior of a polymer fiber Bragg grating (PFBG) illuminated with an LED light source and operating over a range of ambient temperatures. Use of the derived model revealed that light absorption in a PMMA fiber Bragg grating, associated with a 0.5–5 mW LED illumination, resulted in up to 400 W/cm^3 of in-fiber heating and a consequent rise in the temperature of a passively cooled PFBG approaching 18 K. The resulting changes in the effective refractive index and the Bragg grating pitch were found to be significant in magnitude but opposite in sign, thus leading to very modest net changes in the Bragg wavelength. Moreover, an analytical thermo-optical model was found to yield Bragg wavelength shifts that are nearly indistinguishable from the more rigorous numerical solution.

References

[1] L. Eldada, L. Shacklette, Advances in polymer integrated optics, IEEE J. Sel. Top. Quantum Electron. 6 (2000) 54–68.
[2] J.-W. Kang, M.-J. Kim, J.-P. Kim, S.-J. Yoo, J.-S. Lee, D.Y. Kim, J.-J. Kim, Polymeric wavelength filters fabricated using holographic surface relief gratings on azobenzene-containing polymer films, Appl. Phys. Lett. 82 (2003) 3823–3825.
[3] H. Zou, K.W. Beeson, L.W. Shacklette, Tunable planar polymer Bragg gratings having exceptionally low polarization sensitivity, J. Lightwave Technol. 21 (2003) 1083–1088.
[4] A. Sato, M. Scepanovic, R.K. Kostuk, Holographic edge-illuminated polymer Bragg gratings for dense wavelength division optical filters at 1550 nm, Appl. Opt. 42 (2003) 778–784.
[5] S. Tang, Y. Tang, J. Colegrove, D.M. Craig, Fast electrooptic Bragg grating couplers for on-chip reconfigurable optical waveguide interconnects, IEEE Photonics Technol. Lett. 16 (2004) 1385–1387.
[6] C.-L. Chen, Elements of Optoelectronics and Fiber Optics, Irwin, Chicago, 1996, pp. 49–55.
[7] Product specification sheets of Mitsubishi DFB laser diodes (online). Available from: <http://www.mitsubishichips.com/Global/common/cfm/eProfile.cfm?FOLDER=/product/opt/laserdiode/optcomld/dfbld>.
[8] Product catalogs of Denselight LEDs (online). Available from: <http://www.denselight.com/products%20SLED%20modules%20&%20box%20catalog.htm>.
[9] T. Erdogan, Fiber grating spectra, J. Lightwave Technol. 15 (1997) 1277–1294.
[10] H. Kogelnik, Coupled wave theory for thick hologram gratings, Bell Syst. Tech. J. 48 (1969) 2909–2947.
[11] H. Kogelnik, C.V. Shank, Coupled-wave theory of distributed feedback lasers, J. Appl. Phys. 43 (1972) 2327–2335.
[12] A. Yariv, Coupled-mode theory for guided-wave optics, IEEE J. Quantum Electron. 9 (1973) 919–933.
[13] K.J. Kim, Thermo-structural influences on optical characteristics of polymer Bragg gratings. Ph.D. Thesis, Department of Mechanical Engineering, University of Maryland, College Park, MD, 2006.
[14] H.Y. Liu, G.D. Peng, P.L. Chu, Thermal stability of gratings in PMMA and CYTOP polymer fibers, Opt. Commun. 24 (2002) 151–156.
[15] G.D. Peng, P.L. Chu, Polymer optical fiber photosensitivities and highly tunable fiber gratings, Fiber Integr. Opt. 19 (2000) 277–293.
[16] Z. Xiong, G.D. Peng, B. Wu, P.L. Chu, Highly tunable Bragg gratings in single-mode polymer optical fibers, IEEE Photonics Technol. Lett. 11 (1999) 352–354.
[17] M.J. Weber, Handbook of Laser Science and Technology Supplement 2: Optical Materials, CRC Press, Boca Raton, FL, 1995, pp. 75–86.
[18] M. Yamada, K. Sakuda, Analysis of almost-periodic distributed slab waveguides via a fundamental matrix approach, Appl. Opt. 26 (1987) 3474–3478.
[19] A. Othonos, K. Kalli, Fiber Bragg Gratings-Fundamentals and Applications in Telecommunications and Sensing, Artech House, Boston, 1999, pp. 149–187.
[20] R. Steenkiste, G. Springer, Strain and Temperature Measurement with Fiber Optic Sensors, Technomic Publishing Company, Lancaster, PA, 1997, pp. 5–9.
[21] M.N. Ozisik, Heat Conduction, John Willey and Sons, New York, 1980, pp. 133–136.
[22] A.D. Kraus, A. Bar-Cohen, Thermal Analysis and Control of Electronic Equipment, Hemisphere Publishing Corp., New York, 1983, pp. 64–68.